

Electromagnetic radii of the nucleon in soft-wall holographic QCD

Kiminad A. Mamo*

Physics Division, Argonne National Laboratory, Argonne, Illinois 60439, USA

Ismail Zahed†

Center for Nuclear Theory, Department of Physics and Astronomy,
Stony Brook University, Stony Brook, New York 11794-3800, USA

(Dated: May 7, 2022)

We revisit the electromagnetic form factors of the proton and neutron in the holographic soft wall model. At low momentum transfer, we show that by matching the nucleon and rho Regge slopes and fixing the nucleon anomalous dimension by the nucleon mass, a perfect match to the world average charge radii from e-p scattering (including the recent small charge radius of the proton measured by the PRad collaboration at JLab) follows. At high momentum transfer, the nucleon anomalous dimension runs up to match the hard scaling rule.

PACS numbers:

I. INTRODUCTION

The nucleon is a composite hadron with quarks and gluons constituents, the stuff at the origin of all hadronic matter. The quarks are charged and their distribution inside a nucleon is captured by the electric and magnetic charge radii, which measure the charge and current distributions respectively. Precision electron scattering and spectroscopic measurements show a stubborn 4% discrepancy, the so-called proton radius puzzle [1–3]. This is a surprising state of affairs given the fundamental nature of the proton.

The proton structure is the quintessential QCD problem, currently addressed using ab-initio lattice simulations [4]. Empirically, the mass of the proton is known with great accuracy, but its fundamental charge radius is not, as shown in Fig. 1. The high precision e-p measurement of 0.879 fm [2] while consistent with the value of 0.877 fm from hydrogen spectroscopy [3], is larger than the reported value of 0.842 fm from muonic hydrogen spectroscopy [1]. Recent atomic measurements favor smaller radii, while the e-p newest measurements favor larger radii. The exception is the newly released PRad measurement of 0.831 fm at Jefferson Lab [5].

All in all tension seems to exist between e-p scattering measurements of the proton radius and atomic measurements using muonic hydrogen as illustrated in Fig. 1. Although ideas beyond the standard model have been suggested to fix the discrepancy [7, 8], none so far has been empirically conclusive. Dispersive analyses have favored smaller electric and magnetic charge radii [9], although it is in general hard to gauge the theoretical uncertainties given the strong coupling nature of the problem.

The proton structure emerges from a subtle interplay between the sources composing the nucleon and the pri-

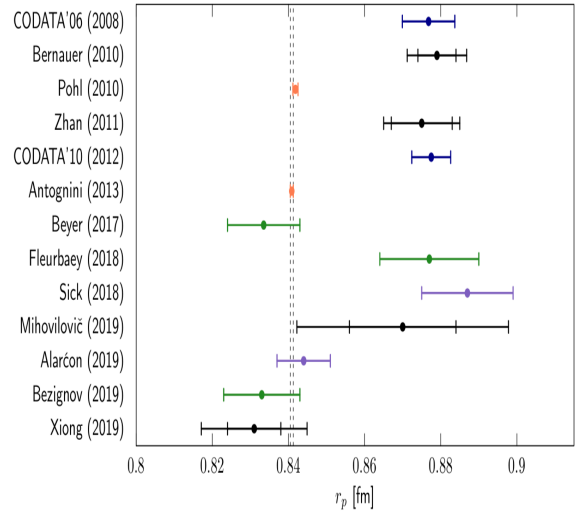


FIG. 1: Sample of measured proton charged radii from atomic (left) and e-p scattering (right) from [6] (and references therein).

mordial glue in the vacuum [10]. Most of the proton mass arises from the spontaneous breaking of chiral symmetry, but its moderately large size makes it still susceptible to the effects of confinement, a feature also shared by the vector mesons but not the light and more compact pseu-

*Electronic address: kmamo@anl.gov

†Electronic address: ismail.zahed@stonybrook.edu

doscalar Goldstone bosons. This last observation is further supported by the straight character of the nucleon and rho Regge trajectories and their remarkable parallelism.

We will address the proton and neutron size problem non-perturbatively in the context of holographic QCD, which among other embodies Regge physics, and provides a field theoretical realization for the dual resonance framework [11] postulated decades ago outside the realm of QCD. The approach, originates from a conjecture that observables in strongly coupled and conformal gauge theories in the limit of a large number of colors and strong gauge coupling, can be determined from classical fields interacting through gravity in an anti-de-Sitter space in higher dimensions [12, 13]. The conjecture has been extended since to non-conformal gauge theories [14].

The holographic description of the electromagnetic form factors in the context of the soft wall model was initially addressed in [15] with rather large electromagnetic radii. Here we show how to overcome this major shortcoming by suggesting that the nucleon anomalous dimension runs with a smaller dimension at low energy that asymptotes its hard scaling value at high energy [16]. The results are much improved electromagnetic radii and form factors at low energy.

The organization of the paper is as follows: in section II we briefly review the derivation of the electromagnetic form factors using the soft wall construction. We propose to use the nucleon mass to fit the nucleon twist factor at low energy, a departure from the standard fit at high energy to reproduce the hard scattering rules. We show that the ensuing electric Sachs form factors are in much better agreement with the e-p world data at small momenta. In section III we extract the electric and magnetic radii of the proton and neutron which are found to be in good agreement with the world averages. In section IV we show that at higher energies the twist factor runs up to reproduce the hard scattering rules in conformity with the resonance dual result. Our conclusions are in V. Details regarding the holographic fields dual to the QCD sources at the boundary are briefly reviewed in the Appendix.

II. ELECTROMAGNETIC FORM FACTORS

The electromagnetic form factors for the nucleon in the context of the soft wall model have been originally addressed in [15], although with a different analysis at low momentum transfer than the one we will present and which will fix the numerical shortcomings they encountered. The form factors can be extracted from the normalized boundary-to-bulk three-point functions with pertinent LSZ reduction

$$W_V^{a\mu}(q^2) = \lim_{p'^2, p^2 \rightarrow m_N^2} (p'^2 - m_N^2)(p^2 - m_N^2) \times \frac{\langle \mathcal{O}_N(-p') J_V^{a\mu}(q) \mathcal{O}_N(p) \rangle}{F_N(p') F_N(p)} \quad (\text{II.1})$$

for the isoscalar $a = 0$ and the isovector $a = 3$ current $J_V^{a\mu}$, with the nucleon source constant $F_N(p) = \langle 0 | \mathcal{O}_N(0) | N(p) \rangle$. Its explicit form will not be needed. The electromagnetic current form factors follow from

$$W_{EM}^\mu(Q^2) = \langle N(p') | J_{EM}^\mu(0) | N(p) \rangle = \frac{1}{3} W_V^{0\mu}(Q^2) + W_V^{3\mu}(Q^2) \quad (\text{II.2})$$

with $q^2 = (p' - p)^2 = -Q^2$ (space-like). Here $N(p)$ refers to the U(2) proton-neutron doublet.

The vector currents $J_V^{a\mu}$ at the boundary are sourced by the dual bulk vector fields $V_\mu^a(Q, z \rightarrow 0)$. The Dirac and Pauli contributions to the direct part of the electromagnetic current can be extracted from the pertinent bulk Dirac and Pauli parts of the action in the soft wall model. Here and for simplicity, we will detail the extraction for the Dirac contribution and quote the answer for the Pauli one. With this in mind, the Dirac part of the action in (A.16) yields

$$\begin{aligned} S_{Dirac}^{EM}[i, X] = & \frac{1}{2g_5^2} \int dz d^4y \sqrt{-\bar{\kappa}} e^{-\bar{\kappa}^2 z^2} \frac{z}{R} \\ & \times \left(\bar{\Psi}_{1X} \gamma^N \left(\frac{1}{3} V_N^0 T^0 + V_N^3 T^3 \right) \Psi_{1i} + \bar{\Psi}_{2X} \gamma^N \left(\frac{1}{3} V_N^0 T^0 + V_N^3 T^3 \right) \Psi_{2i} \right), \\ = & (2\pi)^4 \delta^4(P_X - p - q) \times F_X(P_X) \times F_N(p) \\ & \times \frac{1}{2g_5^2} \times 2g_5^2 \times e_N \times \bar{u}_{s_X}(P_X) \epsilon(q) u_{s_i}(p) \times \frac{1}{2} \left[\mathcal{I}_L(n_X, Q^2) + \mathcal{I}_R(n_X, Q^2) \right], \end{aligned} \quad (\text{II.3})$$

following the conventions in [17]. Here $\epsilon^\mu(q)$ is the polarization of the electromagnetic (EM) probe. In the last equality in (II.3) we substituted the bulk gauge fields by (A.5), and the bulk fermionic currents in terms of the fermionic fields (A.11). The charge assignments are $e_N = 1$ for the proton, and $e_N = 0$ for the neutron. We have also defined

$$\mathcal{I}_L(n_X, Q^2) \equiv \mathcal{I}(M + 5/2, n_X, Q^2) \quad \mathcal{I}_R(n_X, Q^2) \equiv \mathcal{I}(M + 3/2, n_X, Q^2) \quad (\text{II.4})$$

with

$$\mathcal{I}(\bar{m}, n_X, Q^2) = \frac{\Gamma(\bar{m})}{\Gamma(\bar{m}-1)} \left(\frac{\Gamma(\bar{m}-1) \Gamma(n_X + \bar{m}-1)}{\Gamma(n_X+1)} \right)^{\frac{1}{2}} \frac{\frac{Q^2}{4\tilde{\kappa}^2} \Gamma\left(\frac{Q^2}{4\tilde{\kappa}^2} + n_X\right)}{\Gamma\left(\frac{Q^2}{4\tilde{\kappa}^2} + n_X + \bar{m}\right)} \quad (\text{II.5})$$

We made use of the final state mass shell condition

$$P_X^2 = M_X^2 = (p+q)^2 = m_N^2 + Q^2 \left(\frac{1}{x} - 1 \right) = 4\tilde{\kappa}^2 \left(n_X + M + \frac{1}{2} \right) \quad (\text{II.6})$$

with the identification $n_X = Q^2(1/x-1)/4\tilde{\kappa}^2$ and $M \equiv \tau - 3/2$. For the initial state we have $p^2 = m_N^2 = 4\tilde{\kappa}^2(M+1/2)$. The Dirac part of the electromagnetic current (II.2) follows from (II.3) by variation

$$W_{EM(Dirac)}^\mu(Q^2) = \bar{u}_{s'}(p') \gamma^\mu u_s(p) \times e_N \times C_1(Q) \equiv \frac{1}{F_N(p') F_N(p)} \frac{\delta S_{Dirac}^{EM}}{\delta \epsilon_\mu(q)} \quad (\text{II.7})$$

or more explicitly

$$C_1(Q) = \frac{1}{2} \left[\mathcal{I}_L(n_X = 0, Q^2) + \mathcal{I}_R(n_X = 0, Q^2) \right] \equiv \frac{1}{2} \int \frac{dz}{z^{2M}} e^{-\phi} \mathcal{V}(Q, z) (\psi_L^2(z) + \psi_R^2(z)) . \quad (\text{II.8})$$

with $\phi = \tilde{\kappa}^2 z^2$. The nucleon (ground state) bulk wave functions are given by (A.11)

$$\begin{aligned} \psi_R(z) &= \tilde{n}_R \xi^{\tau - \frac{3}{2}} L_0^{(\tau-2)}(\xi) \equiv \tilde{n}_R \xi^{\tau - \frac{3}{2}}, \\ \psi_L(z) &= \tilde{n}_L \xi^{\tau-1} L_0^{(\tau-1)}(\xi) \equiv \tilde{n}_L \xi^{\tau-1}, \end{aligned} \quad (\text{II.9})$$

with the generalized Laguerre polynomials $L_n^{(\alpha)}(\xi)$, $\xi = \tilde{\kappa}^2 z^2$, $\tilde{n}_R = \tilde{n}_L \sqrt{\tau-1}$ and $\tilde{n}_L = \tilde{\kappa}^{\tau-2} \sqrt{2/\Gamma(\tau)}$. Note that normalizing $C_1(0) = 1$ for the proton, fixes $1 + \mathcal{O}(N_c^{-2}) = 1$.

The nucleon electromagnetic form factors including the Pauli contribution follows a similar reasoning, with the result for the proton

$$\begin{aligned} F_1^P(Q) &= C_1(Q) + \eta_P C_2(Q), \\ F_2^P(Q) &= \eta_P C_3(Q). \end{aligned} \quad (\text{II.10})$$

and the neutron

$$\begin{aligned} F_1^N(Q) &= \eta_N C_2(Q), \\ F_2^N(Q) &= \eta_N C_3(Q). \end{aligned} \quad (\text{II.11})$$

The additional invariant form factors stem from the Pauli contribution. They are structurally similar to the Dirac one in (II.8), with

$$\begin{aligned} C_2(Q) &= \frac{1}{2} \int \frac{dz}{z^{2M}} e^{-\phi} z \partial_z \mathcal{V}(Q, z) (\psi_L^2(z) - \psi_R^2(z)), \\ C_3(Q) &= 2 \int \frac{dz}{z^{2M}} e^{-\phi} m_N z \mathcal{V}(Q, z) \psi_L(z) \psi_R(z). \end{aligned} \quad (\text{II.12})$$

with $m_N = 2\tilde{\kappa}\sqrt{\tau-1}$. Note that the contributions $C_{1,2}$ to the Dirac form factors are chirality-spin preserving with LL and RR following the γ^μ assignment, while the contribution C_3 to the Pauli form factor is chirality-spin flipping with LR following the $\sigma^{\mu\nu}$ assignment. The non-normalizable solution in bulk to the U(1) gauge field, is the bulk-to-boundary vector propagator

$$\mathcal{V}(Q, z) = \xi \Gamma(1+a) \mathcal{U}(1+a; 2; \xi) = \xi \int_0^1 \frac{dx}{(1-x)^2} x^a \exp\left(-\frac{x \xi}{1-x}\right), \quad (\text{II.13})$$

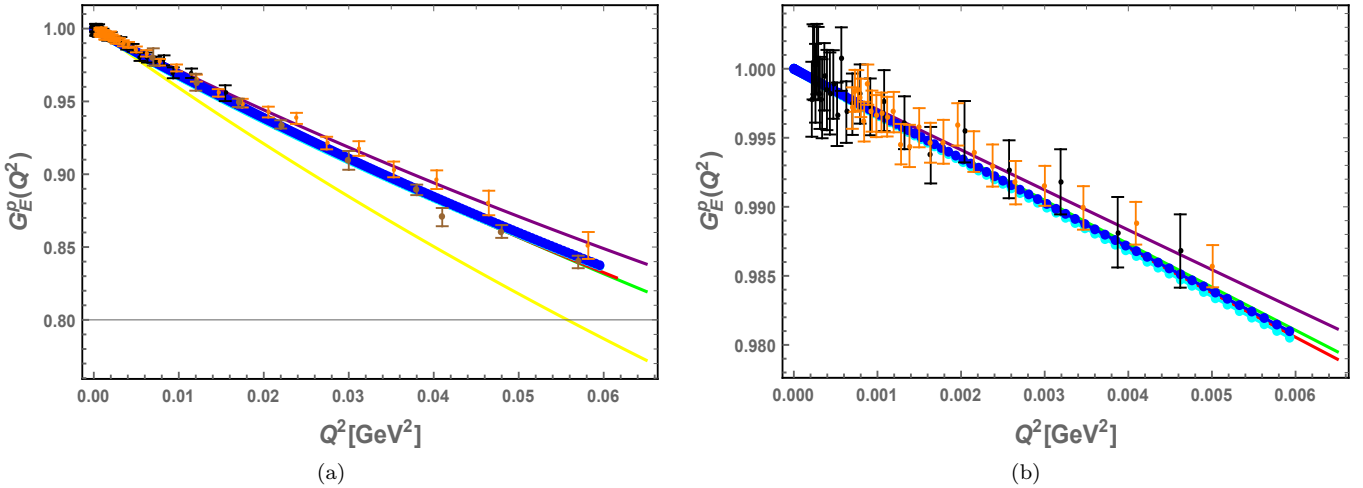


FIG. 2: Sachs electric form factor at low momentum transfer. The green-solid curve is our soft-wall AdS/QCD result with $\tau = m_N^2/m_\rho^2 + 1$ and $4\tilde{\kappa}^2 = m_\rho^2$. The yellow-solid curve is the soft-wall AdS/QCD result for $\tau = 3$ and $\tilde{\kappa} = 0.350$ GeV [15]. The solid-purple curve is the fit to PRad data [5] (orange and black data points). The solid-red curve is the Arrington fit to world data [18] (brown data points). The connected-dotted-blue and the connected-dotted-cyan lines are the most flexible spline and polynomial fits to the Mainz data [19], respectively.

with $a = Q^2/(4\tilde{\kappa}^2)$ and $\xi = \tilde{\kappa}^2 z^2$, and satisfies $\mathcal{V}(0, z) = \mathcal{V}(Q, 0) = 1$. For small momenta $a \ll 1$ it can be expanded

$$\begin{aligned} \mathcal{V}(Q, z) &= \xi \int_0^1 \frac{dx}{(1-x)^2} e^{-\frac{\xi x}{1-x}} \left(1 + a \log(x) \right. \\ &\quad \left. + \frac{1}{2} a^2 \log^2(x) + \mathcal{O}(a^3) \right) \end{aligned} \quad (\text{II.14})$$

The additional coefficients $\eta_{P,N} = 2g_5^2 \times (\eta_3 \pm \eta_0)/2$ in (II.10-II.11) follow from the extra couplings $\eta_{0,3}$ for the singlet and triplet contributions of the bulk Pauli contribution [15]. The Pauli parameter of the proton η_P can be determined by matching the value of $F_2^P(0)$ with the experimental data which is 1.793. For the neutron, the Pauli parameter of the neutron η_N can be determined by matching the value of $F_2^N(0)$ with the experimental data which is -1.913. For $\tau = m_N^2/m_\rho^2 + 1$ and $4\tilde{\kappa}^2 = m_\rho^2$, we have $\eta_P = 0.423$ and $\eta_N = -0.452$.

The standard electric and magnetic Sachs form factors for the proton and neutron are given by

$$\begin{aligned} G_E^{P,N}(Q) &= F_1^{P,N}(Q) - \frac{Q^2}{4m_N^2} F_2^{P,N}(Q) \\ G_M^{P,N}(Q) &= F_1^{P,N}(Q) + F_2^{P,N}(Q) \end{aligned} \quad (\text{II.15})$$

In Fig. 2 we show the electric Sachs form factor. The solid-green curve is our soft-wall prediction for $\tau = m_N^2/m_\rho^2 + 1$ and $4\tilde{\kappa}^2 = m_\rho^2$. The solid-yellow curve is the soft-wall prediction for $\tau = 3$ and $\tilde{\kappa} = 0.350$ GeV. The solid-purple curve is the fit to the PRad data [5] (orange and black data points). The solid-red curve is

the Arrington fit to world data [18] (brown data points). The connected-dotted-blue and the connected-dotted-cyan lines (almost undistinguishable) are the most flexible spline and polynomial fits to the Mainz data [19], respectively. Note that the holographic solid-green curve is undistinguishable from the Arrington and Mainz fits.

III. ELECTROMAGNETIC RADII

A. Proton

The charge radius for the proton is given by

$$\langle r_C^2 \rangle_p = -6 \left(\frac{d \ln G_E^P(Q)}{dQ^2} \right)_0, \quad (\text{III.16})$$

with explicitly

$$\langle r_C^2 \rangle_p (\tau, \tilde{\kappa}) = \frac{C_{Ep}(\tau)}{4\tilde{\kappa}^2}, \quad (\text{III.17})$$

and

$$\begin{aligned} C_{Ep}(\tau) &= \frac{2.69}{\tau - 1} - \frac{3}{\tau} \\ &\quad + \frac{(10.752(\tau - 1) - 5.376)\Gamma(2(\tau - 1))}{\Gamma(2\tau)} + 6\psi(\tau + 1) + 6\gamma, \end{aligned} \quad (\text{III.18})$$

Here $\psi(z)$ is the digamma function and $\gamma \simeq 0.577216$ is Euler's constant.

We now choose to fix the nucleon and rho slopes through the rho meson mass, $4\tilde{\kappa}^2 = m_\rho^2 = 0.775^2$ GeV 2 or $\tilde{\kappa} = 0.388$ GeV, and the the nucleon twist by the nucleon mass

$$\tau - 1 = \frac{m_N^2}{m_\rho^2} = \frac{0.938^2}{0.775^2} = 1.465$$

Note that the canonical dimension for the QCD baryonic sources is $\Delta = 9/2$ which would suggest a twist $\tau = 4$. However, we expect non-vanishing anomalous dimensions to develop at strong coupling. We do not know of any reliable calculational scheme to assess them. We will assume Δ and thus τ as a parameter that runs with the energy scale, with $\tau = 2.465$ (see below) at low energy that asymptotes $\tau = 3$ at high energy in conformity with the hard scattering rule.

With this in mind, we find the charge radius of the proton to be

$$\langle r_C^2 \rangle_p = \frac{C_{Ep} \left(\frac{m_N^2}{m_\rho^2} + 1 \right)}{m_\rho^2} \hbar^2 c^2 = (0.865 \text{ fm})^2, \quad (\text{III.19})$$

in perfect agreement with the world average of e-p scattering from PRad data (with Rational(1,1) fit) [5], Mainz data (with the average of the most flexible Spline and Polynomial fits) [19], and world data (with Arrington and Sick (2015) world updated value [20]), respectively, which is $\langle r_C^2 \rangle_p^{\frac{1}{2}} = (0.831 \text{ fm} + 0.879 \text{ fm} + 0.881 \text{ fm})/3 = 0.864 \text{ fm}$, see Fig. 2.

The magnetic radius for the proton is defined as

$$\langle r_M^2 \rangle_p = -6 \left(\frac{d \ln G_M^P(Q)}{dQ^2} \right)_0, \quad (\text{III.20})$$

with the holographic result

$$\langle r_M^2 \rangle_p(\tau, \tilde{\kappa}) = \frac{C_{Mp}(\tau)}{4\tilde{\kappa}^2}, \quad (\text{III.21})$$

and

$$\begin{aligned} C_{Mp}(\tau) &= \frac{6}{\Gamma(2\tau)(1.793\Gamma(\tau+1) + \tau\Gamma(\tau))} \\ &\times (\Gamma(\tau+1)((1.793\tau - 2.69)\Gamma(2(\tau-1)) \\ &+ \Gamma(2\tau)(1.793\psi(2\tau-1) + 1.035)) \\ &+ \Gamma(\tau)\Gamma(2\tau)(\gamma\tau + \tau\psi(\tau+1) - 0.5)). \end{aligned} \quad (\text{III.22})$$

Using the same parameters as we used to calculate the charge radius of the proton, we find the magnetic radius

of the proton to be

$$\langle r_M^2 \rangle_p = \frac{C_{Mp} \left(\frac{m_N^2}{m_\rho^2} + 1 \right)}{m_\rho^2} \hbar^2 c^2 = (0.823 \text{ fm})^2, \quad (\text{III.23})$$

in perfect agreement with the average of e-p scattering Mainz data (with the average of the most flexible Spline and Polynomial fits) [19], and world data (with Arrington and Sick (2015) world updated value [20] or equivalently with the extraction of Zhan, et al. (2011) [21]), respectively, which is $\langle r_M^2 \rangle_p^{\frac{1}{2}} = (0.777 \text{ fm} + 0.867 \text{ fm})/2 = 0.822 \text{ fm}$.

B. Neutron

The charge radius for the neutron is defined as

$$\langle r_C^2 \rangle_n = -6 \left(\frac{d G_E^N(Q)}{dQ^2} \right)_0, \quad (\text{III.24})$$

and is explicitly given by

$$\langle r_C^2 \rangle_n(\tau, \tilde{\kappa}) = -\frac{C_{En}(\tau)}{4\tilde{\kappa}^2}, \quad (\text{III.25})$$

with the proportionality constant defined as

$$C_{En}(\tau) = \frac{2.87}{\tau - 1} + \frac{11.48(\tau - 1.5)\Gamma(2(\tau - 1))}{\Gamma(2\tau)}. \quad (\text{III.26})$$

Using the same parameters as we used to calculate the charge radius of the proton, we find the charge radius of the neutron to be

$$\langle r_C^2 \rangle_n = -\frac{C_{En} \left(\frac{m_N^2}{m_\rho^2} + 1 \right)}{m_\rho^2} \hbar^2 c^2 = -0.189 \text{ fm}^2, \quad (\text{III.27})$$

in fair agreement with the average of MAMI, JLab/Hall-A, and CLAS experiments (with H. Atac, et al. (2021) fit [22]), and world data (with Kelly (2004) fit [23]), which is $\langle r_C^2 \rangle_n^{\frac{1}{2}} = (-0.110 \text{ fm}^2 - 0.112 \text{ fm}^2)/2 = -0.111 \text{ fm}^2$.

Finally, the magnetic radius for the neutron is defined as

$$\langle r_M^2 \rangle_n = -6 \left(\frac{d \ln G_M^N(Q)}{dQ^2} \right)_0, \quad (\text{III.28})$$

with

$$\langle r_M^2 \rangle_n(\tau, \tilde{\kappa}) = \frac{C_{Mn}(\tau)}{4\tilde{\kappa}^2}, \quad (\text{III.29})$$

and the proportionality constant defined as

$$\begin{aligned} C_{Mn}(\tau) &\equiv \frac{6(\tau - 1.5)\Gamma(2(\tau - 1))}{\Gamma(2\tau)} \\ &+ 6(\psi(2\tau - 1) + 0.577). \end{aligned} \quad (\text{III.30})$$

Using the same parameters as we used to calculate the

charge radius of the proton, we find the magnetic radius of the neutron to be

$$\langle r_M^2 \rangle_n = \frac{C_{Mn} \left(\frac{m_N^2}{m_\rho^2} + 1 \right)}{m_\rho^2} \hbar^2 c^2 = (0.859 \text{ fm})^2, \quad (\text{III.31})$$

in good agreement with the PDG world average [24] $\langle r_M^2 \rangle_n^{\frac{1}{2}} = 0.864 \text{ fm}$. We have summarized our results and comparison to experiment in Table 1.

TABLE I: Comparison of the soft-wall holographic QCD electromagnetic radii of the nucleons with experiment, using $\tau = m_N^2/m_\rho^2 + 1$ and $4\tilde{\kappa}^2 = m_\rho^2$. See text for the references for the quoted experimental values.

Nucleon radii	Experimental values	Soft-wall AdS/QCD [This work]
$\sqrt{\langle r_E^p \rangle^2}$	0.864 fm (e-p world average)	0.865 fm
$\sqrt{\langle r_E^p \rangle^2}$	0.841 fm (μp Lamb shift)	0.865 fm
$\sqrt{\langle r_M^p \rangle^2}$	0.822 fm (e-p world average)	0.823 fm
$\langle (r_E^n)^2 \rangle$	-0.111 fm ² (world average)	-0.189 fm ²
$\sqrt{\langle r_M^n \rangle^2}$	0.864 fm (PDG world average)	0.859 fm

IV. HARD SCATTERING RULE AND THE DUAL RESONANCE MODEL

The hard scaling behavior for the electric form factor [16] is recovered at high energy by allowing τ to run up $\tau = 2.465 \rightarrow 3$. To show this, we note that the contribution $C_1(Q)$ to the Dirac form factor in (II.10) evaluates exactly to

$$C_1(Q) = \frac{a}{2} \left(B(\tau + 1, a) + B(\tau, a + 1) \right) = aB(\tau, a) \quad (\text{IV.32})$$

with $a = Q^2/4\tilde{\kappa}^2$ and $B(x, y)$ the symmetric Euler beta-function. At high momentum with $a \gg 1$ and fixed τ , (IV.32) asymptotes

$$C_1(Q) = aB(\tau, a) \approx \frac{\Gamma(\tau)}{a^{\tau-1}} \quad (\text{IV.33})$$

in agreement with the hard scattering rule for $\tau = 3$. This scaling law originates from the contribution of the R-spinor (II.9) in the form factor near the UV boundary, as it dwarfs that of the L-spinor (II.9) when inserted in the integral (II.8), with the bulk-to-boundary propagator

$\mathcal{V}(Q, z \sim 1/Q) \approx 1$. More specifically, the integrand in (II.8) gives

$$\left(\frac{z}{z^{2M}} \right) \times \xi^{2\tau-3} (1 + \xi) \approx \frac{z^{4\tau-6}}{z^{2\tau-4}} \approx \left(\frac{1}{Q^2} \right)^{\tau-1} \quad (\text{IV.34})$$

Note that the Pauli contributions in (II.12) carry integrands with extra $z \sim 1/Q$ suppression near the UV boundary, and are subleading in $1/Q^2$. This is expected since the Pauli term is helicity-flipping.

Finally we note that the Dirac form factor (IV.32) can be re-written as the ratio of two Euler beta-functions

$$C_1(Q) = \frac{B(\tau - 1, \alpha_t)}{B(\tau - 1, \alpha_0)} \quad (\text{IV.35})$$

with the Regge trajectory $\alpha_t = 1 + \alpha' t$ and $t = Q^2$, where $\alpha' = 1/4\tilde{\kappa}^2$ is the open string or rho meson Regge slope. (IV.35) is the old dual resonance result [11] with the rho meson intercept off. The correct intercept corresponds to $1 \rightarrow \frac{1}{2}$. Since the dual resonance description is rooted in the Veneziano amplitude for open string scattering, it is not surprising that the holographic description which captures the dominant stringy excitations in bulk, recovers it.

V. CONCLUSIONS

At low momentum transfer, the holographic description of the electric and magnetic form factors of the nucleon in the context of the soft wall model shows much improvement when the nucleon anomalous dimension or twist is set by the nucleon mass spectrum at low momentum transfer, fixing a major shortcoming in [15]. The result is a smaller twist factor or $\tau = 2.345$ with a proton electromagnetic radius in remarkable agreement with the current world averaged e-p scattering data.

At high momentum transfer the twist factor runs up $\tau \rightarrow 3$ to reproduce the hard scattering rules. τ is tied to the probing currents with anomalous dimensions at the boundary. Presently, there is no reliable way to assess these anomalous dimensions at strong coupling. At very high momentum transfer, asymptotic freedom sets in. The anomalous dimensions and scaling follow from weak coupling.

Holography recovers the old dual description with all its phenomenological successes. However, it should be stressed that holography provides much more than that. Indeed, the bulk holographic description in higher dimension allows for the assessment of any n-point function on the boundary through their dual Witten diagrams in bulk, in the double limit of large N_c and strong gauge coupling. It also provides for novel physics for dense systems as dual to black holes in bulk.

Acknowledgments

K.M. is supported by the U.S. Department of Energy, Office of Science, Office of Nuclear Physics, contract no. DE-AC02-06CH11357, and an LDRD initiative at Argonne National Laboratory under Project No. 2020-0020. I.Z. is supported by the Office of Science, U.S. Department of Energy under Contract No. DE-FG-88ER40388.

Appendix A: Soft-wall holographic QCD

A simple way to capture AdS/CFT duality in the non-conformal limit is to model it using a slice of AdS_5 with various bulk fields with assigned anomalous dimensions and pertinent boundary values, in the so-called bottom-up approach which we will follow here using the conventions in our recent work in DIS scattering [25, 26]. We consider AdS_5 with a soft wall with a background metric $g_{MN} = (\eta_{\mu\nu}, -1)R^2/z^2$ with the flat metric $\eta_{\mu\nu} = (1, -1, -1, -1)$ at the boundary. Confinement will be described by a harmonic background dilaton $\phi = \tilde{\kappa}^2 z^2$.

1. Bulk vector mesons

The vector mesons fields L, R are described by the bulk effective action [27, 28]

$$S_M = -\frac{1}{4g_5^2} \int d^5x e^{-\phi(z)} \sqrt{g} g^{MP} g^{NQ} \text{Tr} \left(\mathcal{F}_{MN}^L \mathcal{F}_{PQ}^L + \mathcal{F}_{MN}^R \mathcal{F}_{PQ}^R \right) + \int d^5x \left(\omega_5^L(\mathcal{A}) - \omega_5^R(\mathcal{A}) \right) \quad (\text{A.1})$$

with the Chern-Simons contribution

$$\omega_5(\mathcal{A}) = \frac{N_c}{24\pi^2} \int d^5x \text{Tr} \left(\mathcal{A} \mathcal{F}^2 + \frac{1}{2} \mathcal{A}^3 \mathcal{F} - \frac{1}{10} \mathcal{A}^5 \right) \quad (\text{A.2})$$

Here $\mathcal{F} = d\mathcal{A} - i\mathcal{A}^2$ and $\mathcal{A} = \mathcal{A}^a T^a$ with $T^0 = \frac{3}{2}\mathbf{1}_2$ and $T^i = \frac{1}{2}\tau^i$, with the form notation subsumed. Also the vector fields are given by $V = (R + L)/2$ and the axial-vector fields are given by $A = (R - L)/2$. The coupling g_5 in (A.1) is fixed by the brane embeddings in bulk, or phenomenologically as $1/g_5^2 \equiv N_c/(12\pi^2)$ [29].

The flavor gauge fields solve

$$\square V^\mu + ze^{\tilde{\kappa}^2 z^2} \partial_z \left(e^{-\tilde{\kappa}^2 z^2} \frac{1}{z} \partial_z V^\mu \right) = 0 \quad \square V_z - \partial_z \left(\partial_\mu V^\mu \right) = 0. \quad (\text{A.3})$$

subject to the gauge condition

$$\partial_\mu V^\mu + ze^{\kappa^2 z^2} \partial_z \left(e^{-\kappa^2 z^2} \frac{1}{z} V_z \right) = 0, \quad (\text{A.4})$$

with the boundary condition $V_\mu(z, y)|_{z \rightarrow 0} = \epsilon_\mu(q) e^{-iq \cdot y}$. The non-normalizable solutions are

$$\begin{aligned}
V_\mu(z, y) &= \epsilon_\mu(q) e^{-iq \cdot y} \Gamma\left(1 + \frac{Q^2}{4\tilde{\kappa}^2}\right) \tilde{\kappa}^2 z^2 \mathcal{U}\left(1 + \frac{Q^2}{4\tilde{\kappa}^2}; 2; \tilde{\kappa}^2 z^2\right) \\
V_z(z, y) &= \frac{i}{2} \epsilon(q) \cdot q e^{-iq \cdot y} \Gamma\left(1 + \frac{Q^2}{4\tilde{\kappa}^2}\right) z \mathcal{U}\left(1 + \frac{Q^2}{4\tilde{\kappa}^2}; 1; \tilde{\kappa}^2 z^2\right),
\end{aligned} \tag{A.5}$$

with $\mathcal{U}(a; b; w)$ the confluent hypergeometric functions of the second kind.

2. Bulk Dirac fermions

The bulk Dirac fermion action in a sliced of AdS_5 is

$$S_F = \frac{1}{2g_5^2} \int d^5x e^{-\phi(z)} \sqrt{g} \left(\mathcal{L}_{F1} + \mathcal{L}_{F2} \right) + \frac{1}{2g_5^2} \int d^4x \sqrt{-g^{(4)}} \left(\mathcal{L}_{UV1} + \mathcal{L}_{UV2} \right), \tag{A.6}$$

The Dirac and Pauli contributions to $\mathcal{L}_{F1,2}$ are respectively

$$\begin{aligned}
\mathcal{L}_{\text{Dirac}1,2} &= \left(\frac{i}{2} \bar{\Psi}_{1,2} e_A^N \Gamma^A (\vec{D}_N^{L,R} - \overleftarrow{D}_N^{L,R}) \Psi_{1,2} - (\pm M + V(z)) \bar{\Psi}_{1,2} \Psi_{1,2} \right), \\
\mathcal{L}_{\text{Pauli}1,2} &= \pm 2g_5^2 \times \eta \bar{\Psi}_{1,2} e_A^M e_B^N \sigma^{AB} \mathcal{F}_{MN}^{L,R} \Psi_{1,2},
\end{aligned} \tag{A.7}$$

with $V(z) = \tilde{\kappa}^2 z^2$, $e_A^N = z \delta_A^N$, $\sigma^{AB} = \frac{i}{2} [\Gamma^A, \Gamma^B]$, and $\omega_{\mu z \nu} = -\omega_{\mu \nu z} = \frac{1}{z} \eta_{\mu \nu}$. The Dirac gamma matrices $\Gamma^A = (\gamma^\mu, -i\gamma^5)$ are chosen in the chiral representation. They satisfy the flat anti-commutation relation $\{\Gamma^A, \Gamma^B\} = 2\eta^{AB}$. The left and right covariant derivatives are defined as

$$\begin{aligned}
\vec{D}_N^{X=L,R} &= \vec{\partial}_N + \frac{1}{8} \omega_{NAB} [\Gamma^A, \Gamma^B] - iX_N^a T^a \equiv \vec{\mathcal{D}}_N - iX_N^a T^a \\
\overleftarrow{D}_N^{X=L,R} &= \overleftarrow{\partial}_N + \frac{1}{8} \omega_{NAB} [\Gamma^A, \Gamma^B] + iX_N^a T^a \equiv \overleftarrow{\mathcal{D}}_N + iX_N^a T^a
\end{aligned} \tag{A.8}$$

The nucleon doublet refers to

$$\Psi_{1,2} \equiv \begin{pmatrix} \Psi_{p1,2} \\ \Psi_{n1,2} \end{pmatrix}. \tag{A.9}$$

The nucleon fields in bulk form an iso-doublet p, n with $1, 2$ referring to their boundary chirality $1, 2 = \pm = R, L$ [30]. They are dual to the boundary sources $\Psi_{p1,2} \leftrightarrow \mathcal{O}_{p,\pm}$ and $\Psi_{n1,2} \leftrightarrow \mathcal{O}_{n,\pm}$ with anomalous dimensions $\pm M = \pm(\Delta - 2) = \pm(\tau - 3/2)$.

The equation of motions for the bulk Dirac chiral doublet is

$$\left(ie_A^N \Gamma^A D_N^{L,R} - \frac{i}{2} (\partial_N \phi) e_A^N \Gamma^A - (\pm M + V(z)) \right) \Psi_{1,2} = 0, \tag{A.10}$$

The normalizable solution to (A.10) are

$$\begin{aligned}
\Psi_1(p, z) &= \psi_R(z) \Psi_R^0(p) + \psi_L(z) \Psi_L^0(p) \\
\Psi_2(p, z) &= \psi_R(z) \Psi_L^0(p) + \psi_L(z) \Psi_R^0(p)
\end{aligned} \tag{A.11}$$

with the normalized bulk wave functions

$$\begin{aligned}\psi_R(z) &= \tilde{n}_R \xi^{\tau - \frac{3}{2}} L_n^{(\tau-2)}(\xi) = \frac{\tilde{n}_R}{\tilde{\kappa}^{\tau-2}} z^{\frac{5}{2}} \xi^{\frac{\tau-2}{2}} L_n^{(\tau-2)}(\xi), \\ \psi_L(z) &= \tilde{n}_L \xi^{\tau-1} L_n^{(\tau-1)}(\xi) = \frac{\tilde{n}_L}{\tilde{\kappa}^{\tau-1}} z^{\frac{5}{2}} \xi^{\frac{\tau-1}{2}} L_n^{(\tau-1)}(\xi),\end{aligned}\tag{A.12}$$

Here $\xi = \tilde{\kappa}^2 z^2$, $L_n^{(\alpha)}(\xi)$, $\tilde{n}_R = \tilde{n}_L \tilde{\kappa}^{-1} \sqrt{\tau - 1}$ are the generalized Laguerre, and $\tilde{n}_L = \tilde{\kappa}^\tau \sqrt{2/\Gamma(\tau)}$. The free Weyl spinors $\Psi_{R/L}^0(p) = P_\pm u(p)$ and $\bar{\Psi}_{R/L}^0(p) = \bar{u}(p) P_\mp$, and the free boundary spinors satisfy

$$2m_N \times \bar{u}(p')\gamma^\mu u(p) = \bar{u}(p')(p' + p)^\mu u(p). \quad (\text{A.13})$$

The fermionic spectrum Reggeizes $m_n^2 = 4\tilde{\kappa}^2(n + \tau - 1)$. The assignments $1 = +$ and $2 = -$ at the boundary are commensurate with the substitutions $\psi_{R,L} \leftrightarrow \mp \psi_{L,R}$ by parity.

Using the Dirac 1-form currents

$$\begin{aligned} J_L^{aN} &= \frac{\partial \mathcal{L}_{\text{Dirac1}}}{\partial L_N^a} = \bar{\Psi}_1 e_A^N \Gamma^A T^a \Psi_1, \\ J_R^{aN} &= \frac{\partial \mathcal{L}_{\text{Dirac2}}}{\partial R_N^a} = \bar{\Psi}_2 e_A^N \Gamma^A T^a \Psi_2, \end{aligned} \quad (\text{A.14})$$

and Pauli 2-form currents

$$\begin{aligned} J_L^{aMN} &= \frac{\partial \mathcal{L}_{\text{Pauli1}}}{\partial L_{MN}^a} = +2g_5^2 \times \eta^a \bar{\Psi}_1 e_A^M e_B^N \sigma^{AB} T^a \Psi_1, \\ J_R^{aMN} &= \frac{\partial \mathcal{L}_{\text{Pauli2}}}{\partial R_{MN}^a} = -2g_5^2 \times \eta^a \bar{\Psi}_2 e_A^M e_B^N \sigma^{AB} T^a \Psi_2. \end{aligned} \quad (\text{A.15})$$

we can rewrite (A.7) with the explicit isoscalar ($a = 0$) and isovector ($a = 3$) contributions

$$\begin{aligned} \mathcal{L}_{F1} + \mathcal{L}_{F2} \supset & \frac{i}{2} \bar{\Psi}_1 e_A^N \Gamma^A (\vec{\mathcal{D}}_N - \overleftarrow{\mathcal{D}}_N) \Psi_1 - (M + V(z)) \bar{\Psi}_1 \Psi_1 + \frac{i}{2} \bar{\Psi}_2 e_A^N \Gamma^A (\vec{\mathcal{D}}_N - \overleftarrow{\mathcal{D}}_N) \Psi_2 - (-M + V(z)) \bar{\Psi}_2 \Psi_2 \\ & + V_N^0 J_V^{0N} + A_N^0 J_A^{0N} + V_N^3 J_V^{3N} + A_N^3 J_A^{3N} + V_{MN}^0 J_V^{0MN} + A_{MN}^0 J_A^{0MN} + V_{MN}^3 J_V^{3MN} + A_{MN}^3 J_A^{3MN} \end{aligned} \quad (\text{A.16})$$

with $J_{V,A}^{aN} = J_L^{aN} \pm J_R^{aN}$ and $J_{V,A}^{aMN} = J_L^{aMN} \mp J_R^{aMN}$.

- [1] R. Pohl et al., *Nature* **466**, 213 (2010).
- [2] J. C. Bernauer et al. (A1), *Phys. Rev. Lett.* **105**, 242001 (2010), 1007.5076.
- [3] P. J. Mohr, B. N. Taylor, and D. B. Newell, *Rev. Mod. Phys.* **84**, 1527 (2012), 1203.5425.
- [4] S. Durr et al., *Science* **322**, 1224 (2008), 0906.3599.
- [5] W. Xiong et al., *Nature* **575**, 147 (2019).
- [6] J. C. Bernauer, *EPJ Web Conf.* **234**, 01001 (2020).
- [7] A. J. Krasznahorkay et al., *Phys. Rev. Lett.* **116**, 042501 (2016), 1504.01527.
- [8] C. E. Carlson and B. C. Rislow, *Phys. Rev. D* **86**, 035013 (2012), 1206.3587.
- [9] Y.-H. Lin, H.-W. Hammer, and U.-G. Meißner, *Phys. Lett. B* **816**, 136254 (2021), 2102.11642.
- [10] I. Zahed (2021), 2102.08191.
- [11] P. H. Frampton, *Phys. Rev. D* **1**, 3141 (1970).
- [12] J. M. Maldacena, *Adv. Theor. Math. Phys.* **2**, 231 (1998), hep-th/9711200.
- [13] O. Aharony, S. S. Gubser, J. M. Maldacena, H. Ooguri, and Y. Oz, *Phys. Rept.* **323**, 183 (2000), hep-th/9905111.
- [14] E. Witten, *Adv. Theor. Math. Phys.* **2**, 505 (1998), hep-th/9803131.
- [15] Z. Abidin and C. E. Carlson, *Phys. Rev. D* **79**, 115003 (2009), 0903.4818.
- [16] G. P. Lepage and S. J. Brodsky, *Phys. Rev. D* **22**, 2157 (1980).

- [17] C. A. Ballon Bayona, H. Boschi-Filho, and N. R. F. Braga, JHEP **03**, 064 (2008), 0711.0221.
- [18] J. Arrington, W. Melnitchouk, and J. A. Tjon, Phys. Rev. C **76**, 035205 (2007), 0707.1861.
- [19] J. C. Bernauer et al. (A1), Phys. Rev. C **90**, 015206 (2014), 1307.6227.
- [20] J. Arrington and I. Sick, J. Phys. Chem. Ref. Data **44**, 031204 (2015), 1505.02680.
- [21] X. Zhan et al., Phys. Lett. B **705**, 59 (2011), 1102.0318.
- [22] H. Atac, M. Constantinou, Z. E. Meziani, M. Paolone, and N. Sparveris, Nature Commun. **12**, 1759 (2021), 2103.10840.
- [23] J. J. Kelly, Phys. Rev. C **70**, 068202 (2004).
- [24] P. A. Zyla et al. (Particle Data Group), PTEP **2020**, 083C01 (2020).
- [25] K. A. Mamo and I. Zahed, Phys. Rev. D **101**, 086003 (2020), 1910.04707.
- [26] K. A. Mamo and I. Zahed (2021), 2102.00608.
- [27] J. Hirn and V. Sanz, JHEP **12**, 030 (2005), hep-ph/0507049.
- [28] S. K. Domokos, H. R. Grigoryan, and J. A. Harvey, Phys. Rev. D **80**, 115018 (2009), 0905.1949.
- [29] A. Cherman, T. D. Cohen, and E. S. Werbos, Phys. Rev. C **79**, 045203 (2009), 0804.1096.
- [30] D. K. Hong, T. Inami, and H.-U. Yee, Phys. Lett. B **646**, 165 (2007), hep-ph/0609270.